Atomic short-range order in an $Al_{72}Ni_{18}Fe_{10}$ decagonal quasicrystal studied by anomalous x-ray scattering

2007 J. Phys.: Condens. Matter 19 466201

(http://iopscience.iop.org/0953-8984/19/46/466201)

IOP PUBLISHING JOURNAL OF PHYSICS: CONDENSED MATTER

J. Phys.: Condens. Matter **19** (2007) 466201 (14pp) doi:10.1088/0953-8984/19/46/466201

Atomic short-range order in an $Al_{72}Ni_{18}Fe_{10}$ decagonal quasicrystal studied by anomalous x-ray scattering

Hiroshi Abe[1], Kazuki Yamamoto[2], Sayuri Matsuoka[2] and Yoshie Matsuo[2]

[1] Department of Materials Science and Engineering, National Defense Academy, Yokosuka 239-8686, Japan
[2] Department of Physics, Faculty of Science, Nara Women's University, Nara 630-8263, Japan

Received 29 May 2007, in final form 15 August 2007
Published 23 October 2007
Online at stacks.iop.org/JPhysCM/19/466201

Abstract

Diffuse scattering around Bragg reflections was observed by anomalous x-ray scattering in a single decagonal quasicrystal of $Al_{72}Ni_{18}Fe_{10}$. Intensity modulations of the diffuse scattering were measured for four incident x-ray beam energies. Quantitative analysis of the diffuse scattering data shows the presence of atomic short-range order (SRO) in three kinds of pair-correlation functions: Al–Ni, Ni–Fe and Fe–Al. The SRO diffuse scattering is decomposed into each component by self-consistent calculation. Using Metropolis Monte Carlo simulations, the SRO diffuse scattering is calculated qualitatively using the SRO parameters. Asymmetric distributions of the diffuse scattering were seen along a longitudinal direction, even though the $Al_{72}Ni_{18}Fe_{10}$ quasicrystal has quite small mosaicity.

1. Introduction

The Al–Ni–Fe (ANF) system is well known to contain a decagonal quasicrystalline structure, consisting of two-dimensional quasiperiodic planes stacked along the periodic decagonal axis [1]. The quasicrystal structure in ANF is similar to the $Al_{13}Fe_4$ monoclinic approximant structure [2]. High-resolution electron microscopy (HREM) investigation of $Al_{13}Fe_4$ [3] has shown that it is made of pentagonal arrangements. The centers of the pentagonal atomic columns form a pattern of squashed hexagonal tiles. Hexagonal tiling is orientated in the same direction. The space group of the $Al_{70}Ni_{15}Fe_{15}$ quasicrystal was determined using convergent-beam electron diffraction [4] and found to be noncentrosymmetric $P\bar{1}0m3$. Moreover, weak diffuse streaks were located at the $(2n + 1)/c$ reciprocal space layers, where c is the lattice constant in the periodic direction and n is an integer. This means that the lattice modulation is induced by a $2c$ periodicity. A 2 nm columnar cluster and its arrangement in $Al_{70}Ni_{15}Fe_{15}$ have been observed by dark-field electron microscopy and HREM [5]. Neighboring pentagonal clusters have opposite polarity. On the other hand, the stable $Al_{71.6}Ni_{23.7}Fe_{4.7}$ was a highly ordered quasicrystal, whose space group is $P10_5/mmc$ [6]. By high-angle annular dark-field

scanning transmission electron microscopy (HAADF-STEM) [7], it was proposed that three types of 2 nm clusters exist in $Al_{70}Ni_{15}Fe_{15}$. It was also pointed out that antiphase shifts occur at domain boundaries. In $Al_{71.5}Ni_{23.5}Fe_5$, diffuse scattering was observed in the vicinity of Bragg reflection [8]. The anisotropic distributions of diffuse scattering were attributed to a superposition of both thermal diffuse scattering (TDS) and Huang diffuse scattering (HDS), where HDS is derived from an additional defect. Very recently, Yamamoto *et al* found quasicrystal–approximant phase transitions in $Al_{72}Ni_{18}Fe_{10}$ at high temperature [9].

In addition to TDS and HDS, atomic short-range order (SRO) diffuse scattering appears in crystals and quasicrystals. The anomalous x-ray scattering technique was applied to study SRO in $Fe_{22.5}Ni_{77.5}$ [10]. SRO in FeNi alloys is not observable with conventional x-rays, because the SRO diffuse intensities are proportional to the difference of atomic scattering factor. When the incident x-ray beam energy was selected properly, SRO diffuse scattering disappears by the null Laue method ($f_{Fe} = F_{Ni}$). In fact, TDS contributions were estimated experimentally by the null Laue method at 8 eV. It is also found that diffuse peaks shift drastically at each incident x-ray energy. The anomalous x-ray scattering method was applied to an Al–Ni–Co (ANC) decagonal quasicrystal [11]. It was shown that a pure atomic rearrangement of the average lattice sites occurs without 'random phason strain' in the as-quenched sample. The full width at half maximum (FWHM) of the Bragg reflections did not depend on $|\mathbf{G}^{\perp}|$, where $\mathbf{G}^{\perp}$ is the reciprocal lattice vector in the perpendicular space, while $\mathbf{G}^{\parallel}$ is the reciprocal lattice vector in the physical space. Furthermore, *in situ* observations at high temperature were carried out using anomalous x-ray scattering in $Al_{72}Ni_{20}Co_8$ [12]. It was found that an order–disorder phase transition takes place accompanying 'random phason strain'. For instance, it was shown that weak 'random phason strain' developed gradually below T_c.

The concept of phasons was introduced theoretically in quasicrystals [13]. There are three kinds of phasons classified as follows.

(i) 'Random phason strain': peak broadening of Bragg reflections is caused by nonuniform strains. A phason freezes randomly along the equivalent directions.

(ii) 'Phason strain' generated by a tilt of the physical space in the high-dimensional periodic space. Bragg reflections shift from ideal positions and the peak shifts are linked to a quasicrystal (aperiodic)–approximant (periodic) phase transition.

(iii) 'Phason modes' are explained by the hydrodynamic theory. For instance, a random tiling model [14] was proposed to explain the diffuse scattering, which contains some kind of disorder in the long-range geometry. The shape of phasonic diffuse scattering (PDS) depends on 'phason modes'. As an example, the diffuse scattering studies of icosahedral $Al_{68.2}Pd_{22.8}Mn_9$ were performed using neutron diffraction [15]. Using high-energy resolution, phonon contributions to the diffuse scattering were completely separated from the phason contributions. The experimental results were consistent with the calculated PDS, which is regarded as a precursor phenomenon of a quasicrystal–approximant phase transition. In a decagonal quasicrystal ($Al_{70}Ni_{15}Co_{15}$), anisotropic PDS was observed accompanying the SRO diffuse scattering by anomalous x-ray scattering [16]. In addition, 'random phason strain' was characterized by the peak broadening on $|\mathbf{G}^{\perp}|$. Consequently, both 'phason modes' and 'random phason strain' occurred in $Al_{70}Ni_{15}Co_{15}$.

In this study, we show that the SRO diffuse scattering is the main contribution to diffuse scattering in $Al_{72}Ni_{18}Fe_{10}$. Generally speaking, the zone-centered diffuse scattering contains the SRO diffuse scattering, TDS (thermal diffuse scattering) and PDS in a quasicrystal. Theoretical calculated PDS distributions do not fit with the observed ones. The SRO diffuse scattering was successfully subtracted from the total diffuse scattering by self-consistent

calculation. Anisotropic distributions of the diffuse scattering are qualitatively explained by using the SRO parameters in Metropolis Monte Carlo simulations.

2. Scattering theory

2.1. Diffuse scattering theory for a crystal

Let $\mathbf{Q}$ be the scattered wavevector, defined as $\mathbf{Q} = \mathbf{G} + \mathbf{q}$, where $\mathbf{G}$ is the reciprocal lattice vector. Several kinds of diffuse scattering are considered for conventional crystals: atomic SRO, atomic size effect (SE) from displacements induced by chemical ordering of atoms of disparate size, TDS from phonons and HDS from defects are the main contributions. The total diffuse scattering is thus given by [17]

$$I^{\mathrm{diff}} = I^{\mathrm{SRO}} + I^{\mathrm{SE}} + I^{\mathrm{TDS+HDS}}. \tag{1}$$

The SRO diffuse intensity in a binary alloy system is given by

$$I^{\mathrm{SRO}}(\mathbf{Q}) = x_{\mathrm{A}}x_{\mathrm{B}}|f_{\mathrm{A}} - f_{\mathrm{B}}|^2 \sum_m \alpha_m \exp(\mathrm{i}\mathbf{Q}\cdot\mathbf{R}_m) = x_{\mathrm{A}}x_{\mathrm{B}}|\Delta f|^2\alpha(\mathbf{q}) \tag{2}$$

where $\alpha(\mathbf{q})$ is the Fourier transform of the Warren–Cowley SRO parameters. x_{A} is the concentration of A atoms ($x_{\mathrm{B}} = 1 - x_{\mathrm{A}}$). If we put an A atom at the origin, the SRO parameter on the mth site, α_m, becomes

$$\alpha_m = \frac{\langle\sigma_0^{\mathrm{A}}\sigma_m^{\mathrm{B}}\rangle - x_{\mathrm{A}}x_{\mathrm{B}}}{x_{\mathrm{A}}(\delta_{\mathrm{AB}} - x_{\mathrm{B}})} = 1 - \frac{P_m^{\mathrm{AB}}}{x_{\mathrm{B}}}, \qquad \alpha_0 \equiv 1. \tag{3}$$

$P_m^{\mathrm{AB}} = \langle\sigma_0^{\mathrm{A}}\sigma_m^{\mathrm{B}}\rangle/x_{\mathrm{A}}$ is the conditional probability of a B atom on the mth site given an A atom at the origin.

We can obtain nearly pure thermal and static quadratic and higher-order displacement scattering, $I^{\mathrm{TDS+HDS}}$, which is proportional to the square of the average structure factor, $|\bar{f}|^2$, where $|\bar{f}|$ is given by $|x_{\mathrm{A}}f_{\mathrm{A}} + x_{\mathrm{B}}f_{\mathrm{B}}|$. In general, the expression for the elastic diffuse scattering from a disordered binary alloy is given by

$$I^{\mathrm{diff}}(\mathbf{Q}) = N|\Delta c(\mathbf{q})|^2 \times |\Delta f - \bar{f}\mathbf{Q}\cdot\mathbf{A}(\mathbf{q})|^2, \tag{4}$$

where $\Delta c(\mathbf{q})$ are the Fourier transforms of the concentration fluctuations and $\mathbf{A}(\mathbf{q})$ is the vectorial coupling of the atomic displacements to the concentration. In addition, the linear coupling between concentration and displacement terms in equation (4) is also important in particular cases. This term is the cross term of the amplitude product that contributes to I^{SRO} and $I^{\mathrm{TDS+HDS}}$, and is regarded as both chemical and topological ordering. Therefore, this term, referred to as I^{SE}, is proportional to $\Delta f \times \bar{f}$; the actual equation is more complicated [18]. In general, both TDS [19] and HDS [20] are proportional to q^{-2}. The equations are given by

$$I^{\mathrm{TDS}} \propto k_{\mathrm{B}}T\frac{|\mathbf{Q}|^2(C_{ijk\ell}g_kg_\ell)^{-1}}{q^2}, \tag{5}$$

$$I^{\mathrm{HDS}} \propto \frac{|Q_i(C_{ijk\ell}g_kg_\ell)^{-1}P_{jk}g_k|^2}{q^2}, \tag{6}$$

where g_i is the unit vector of q_i and P_{ij} is the elastic dipole derived from a defect.

As mentioned earlier, a 'null Laue' experiment is important in order to clarify SRO between two atomic species having a small difference in atomic number. By selecting the incident x-ray energy so that $|\Delta f| = |f_{\mathrm{A}} - f_{\mathrm{B}}| \cong 0$, we can then estimate and remove pure $I^{\mathrm{TDS+HDS}}$ by the null Laue method and thereby obtain I^{SRO} and I^{SE}. This is because $\bar{f}$ does not depend much on the incident energies, while Δf is very sensitive to them. In a ternary alloy system, the SRO diffuse intensity of equation (2) is rewritten as

$$I^{\mathrm{SRO}} \propto x_{\mathrm{A}}x_{\mathrm{B}}|f_{\mathrm{A}} - f_{\mathrm{B}}|^2\alpha_{\mathrm{AB}}(\mathbf{q}) + x_{\mathrm{B}}x_C|f_{\mathrm{B}} - f_C|^2\alpha_{\mathrm{BC}}(\mathbf{q}) + x_Cx_{\mathrm{A}}|f_C - f_{\mathrm{A}}|^2\alpha_{\mathrm{CA}}(\mathbf{q}). \tag{7}$$

2.2. Diffuse scattering theory for a decagonal quasicrystal

We focus on the phonon and phason elastic energies in a decagonal quasicrystal. Icosahedral notation for phason softening is described in detail elsewhere [21]. In a decagonal quasicrystal, we describe the structural fluctuations of a disordered state by introducing a phonon displacement field, $\mathbf{u} = (u_1, u_2, u_3)$, and a phason displacement field, $\mathbf{v} = (v_1, v_2)$. Phonon displacements are influenced by phason displacements as $\mathbf{u} \to \mathbf{u} + [C^{-1}]_{\parallel,\parallel} C_{\parallel,\perp}\mathbf{v}$, where $\hat{C}$ is the hydrodynamic elastic matrix given by [22]

$$\hat{C}(\mathbf{q}_\parallel) = \begin{pmatrix} C_{\parallel,\parallel} & C_{\parallel,\perp} \\ C_{\perp,\parallel} & C_{\perp,\perp} \end{pmatrix}. \tag{8}$$

The diffuse scattering is given by

$$I^{\mathrm{diff}}(\mathbf{Q}_\parallel) \propto \left({}^t\mathbf{G}_\parallel, {}^t\mathbf{G}_\perp\right) \hat{C}^{-1}(\mathbf{q}_\parallel) \begin{pmatrix} \mathbf{G}_\parallel \\ \mathbf{G}_\perp \end{pmatrix} \propto F_{\mathrm{thermal}} + F_{\mathrm{phason}}, \tag{9}$$

where

$$F_{\mathrm{thermal}} = {}^t\mathbf{G}_\parallel [C^{-1}]_{\parallel,\parallel} \mathbf{G}_\parallel, \tag{10}$$

$$F_{\mathrm{phason}} = {}^t\Delta\mathbf{G}_\perp (C_{\perp,\perp} - {}^tC_{\parallel,\perp}[C^{-1}]_{\parallel,\parallel} C_{\parallel,\perp})^{-1} \Delta\mathbf{G}_\perp, \tag{11}$$

with $\Delta\mathbf{G}_\perp$ equal to $\mathbf{G}_\perp - {}^tC_{\parallel,\perp}[C^{-1}]_{\parallel,\parallel}\mathbf{G}_\parallel$. Similarly to I^{TDS} and I^{HDS}, equation (9) shows a q^{-2} dependence. The actual components of the C-matrix that includes the periodic direction are expressed as

$$\begin{aligned} C_{\parallel,\parallel} = {} & (\lambda{+}2\mu) \begin{pmatrix} q_1^2 & q_1q_2 & 0 \\ q_2q_1 & q_2^2 & 0 \\ 0 & 0 & 0 \end{pmatrix} + \mu \begin{pmatrix} q_2^2 & -q_1q_2 & 0 \\ -q_2q_1 & q_1^2 & 0 \\ 0 & 0 & 0 \end{pmatrix} + C_1 \begin{pmatrix} q_3^2 & 0 & 0 \\ 0 & q_3^2 & 0 \\ 0 & 0 & q_1^2+q_2^2 \end{pmatrix} \\ & + C_2 \begin{pmatrix} 0 & 0 & 0 \\ 0 & 0 & 0 \\ 0 & 0 & q_3^2 \end{pmatrix} + C_3 \begin{pmatrix} 0 & 0 & q_1q_3 \\ 0 & 0 & q_2q_3 \\ q_3q_1 & q_3q_2 & 0 \end{pmatrix} \end{aligned} \tag{12}$$

$$C_{\perp,\perp} = [K_1(q_1^2+q_2^2) + K_2q_3^2] \begin{pmatrix} 1 & 0 \\ 0 & 1 \end{pmatrix}, \qquad C_{\parallel,\perp} = K' \begin{pmatrix} q_1^2-q_2^2 & -2q_1q_2 \\ -2q_2q_1 & q_2^2-q_1^2 \\ 0 & 0 \end{pmatrix},$$

where parallel components are rewritten as $(\mathbf{q}_\parallel)_i \to q_i$ for simplicity. Here, λ and $\mu(>0)$ are the conventional Lamé coefficients, $C_1(>0)$, $C_2(>0)$ and C_3 are the phonon stiffness constants, K_1 and $K_2(>0)$ are the phonon stiffness constants, and K' is a coupling constant of the phonon–phason mixing. For PDS calculations, the following conditions are also required:

$$\lambda + 2\mu > 0, \qquad \mu K_1 > (K')^2, \qquad (\lambda + 2\mu)K_1 > (K')^2. \tag{13}$$

The phason elastic matrix $C_{\perp,\perp}$ is isotropic for decagonal quasicrystals. However, anisotropic distributions of the diffuse scattering are realized if the phonon–phason coupling is taken into account.

3. Experimental details

In order to investigate the existence of diffuse streaks, we carried out x-ray diffraction experiments on a laboratory conventional diffractometer. Mo radiation, monochromatized by a curved highly orientated pyrolytic graphite (HOPG) (002), was used as the primary beam (wavelength 0.071 07 nm). Oscillation photographs obtained using imaging plates (IPR-420, Mac Science) were taken using a 2 kW x-ray generator (Rigaku).

Anomalous x-ray scattering experiments were performed on the BL-4C of the Photon Factory at the High Energy Accelerator Research Organization in Japan. A vertically focusing

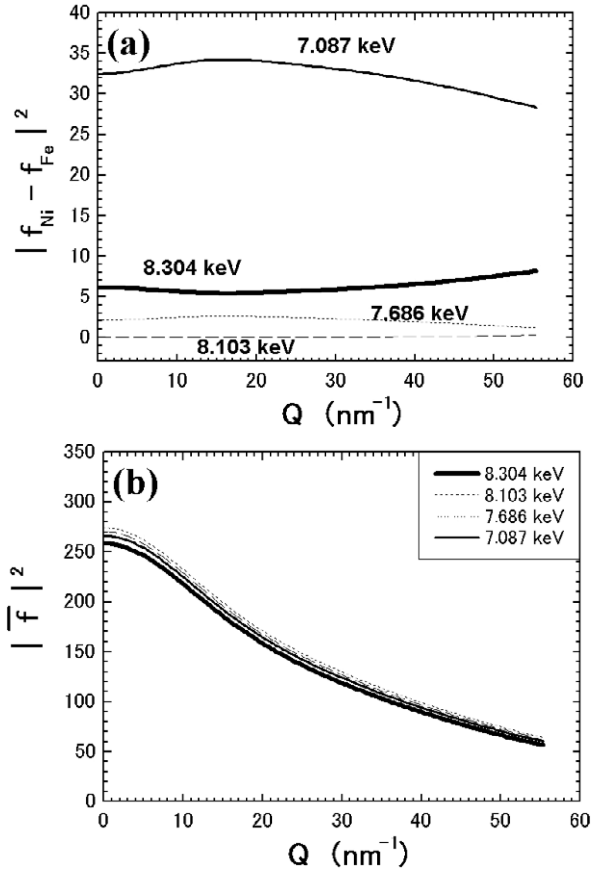

Figure 1. $|\Delta f|^2$ and $|\bar{f}|^2$ as a function of q $(= 4\pi(\sin\theta)/\lambda)$ for the four energies.

mirror was placed in front of a Si(111) double monochromator. The specimen was mounted on a four-circle diffractometer (Huber 5010). Air scattering was minimized by helium-filled beam paths. X-ray fluorescence was removed by a curved HOPG (002). The incident energies were calibrated to within 1 eV using both Ni and Fe foils. Here, we selected the following incident energies: 7.087 keV (near K edge of Fe), 7.686 keV (near K edge of Co), 8.103 keV ($\Delta f \cong 0$) for the 'null Laue' case and 8.304 keV (near K edge of Ni). Figures 1(a) and (b) show the calculated $|\Delta f|^2$ between Ni and Fe and $|\bar{f}|^2$ ($|\bar{f}| = |x_{\mathrm{Al}} f_{\mathrm{Al}} + x_{\mathrm{Ni}} f_{\mathrm{Ni}} + x_{\mathrm{Fe}} f_{\mathrm{Fe}}|$) at each energy, respectively. By anomalous x-ray scattering, we can even obtain the contrast between Ni and Fe, whose difference of atomic number is only two. The Q-resolution of this beam optics is estimated to be around 0.01 nm^{-1} using a Si single crystal. Here, the unit of reciprocal space is $4\pi(\sin\theta)/\lambda$ (nm^{-1}). In order to analyze the diffuse scattering quantitatively (electron units per atom), we measured several integrated intensities of a standard powder sample of Ni at each energy.

An alloy ingot with nominal composition of $Al_{72}Ni_{18}Fe_{10}$ was prepared by melting mixtures of pure Al (99.99%), Ni (99.99%) and Fe (99.99%) metals under an Ar atmosphere in an arc furnace. This ingot was crushed into powder, put into an alumina crucible and then sealed in a quartz tube. The powder sample was melted at 1423 K, slowly cooled to 1073 K at the rate of 50 K h^{-1}, kept at 1073 K for 1 day and then quenched in water ($T_{\mathrm{q}} = 1073$ K). The

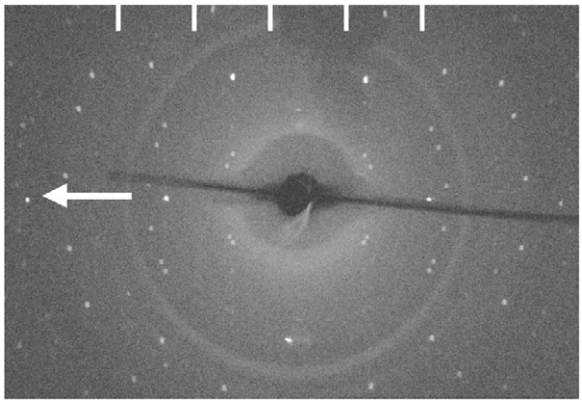

Figure 2. Diffraction pattern of the decagonal quasicrystal $Al_{72}Ni_{18}Fe_{10}$ using an imaging plate. The incident beam is perpendicular to the decagonal axis (c^*-axis).

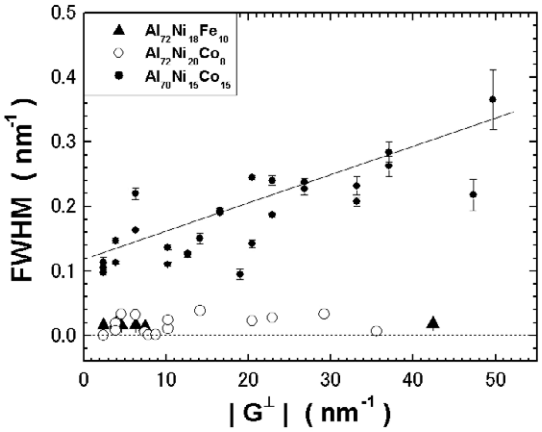

Figure 3. $|\mathbf{G}^{\perp}|$ dependence of FWHM of Bragg reflections. In comparison with that of $Al_{70}Ni_{15}Co_{15}$ and $Al_{72}Ni_{20}Co_8$, no 'random phason strain' was seen in $Al_{72}Ni_{18}Fe_{10}$.

specimen was roughly rod shaped, with a length of 0.071 mm and a diameter of 0.025 mm. It had a mosaicity smaller than 0.02 nm^{-1}. For absorption corrections, we collected equivalent Bragg reflections at each energy. We calculated absorption factors semi-empirically using a numerical scheme.

4. Experimental results

Figure 2 shows an oscillation photograph of $Al_{72}Ni_{18}Fe_{10}$ using an imaging plate. An arrow in figure 2 indicates the c^*-axis. Apparently, no diffuse streaks were seen in $(2n + 1)/2c$ positions, caused by lattice modulation of $2c$ periodicity. In addition, sharp peak spots without additional diffuse scattering were seen in the photograph. This suggests that the sample used in this study is a high-quality quasicrystal. In fact, there is no $|\mathbf{G}^{\perp}|$ dependence of FWHM of Bragg reflections in $Al_{72}Ni_{18}Fe_{10}$ as shown in figure 3. Compared with $Al_{70}Ni_{15}Co_{15}$, it was clear that no 'random phason strain' exists in the as-quenched sample. $Al_{72}Ni_{18}Fe_{10}$ has smaller mosaicity than $Al_{72}Ni_{20}Co_8$ as a perfect quasicrystal.

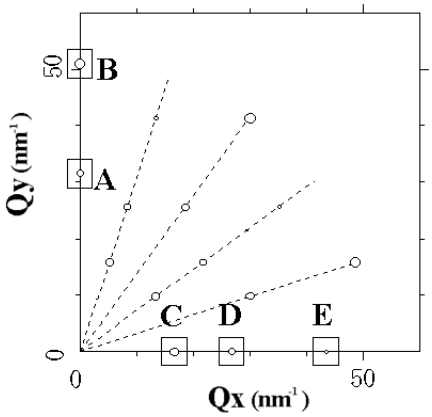

Figure 4. Reciprocal space perpendicular to the periodic direction of the decagonal $Al_{72}Ni_{18}Fe_{10}$ phase. The area of the spot is proportional to the intensity of the reflection. The diffuse scattering has been measured around the labeled reflections.

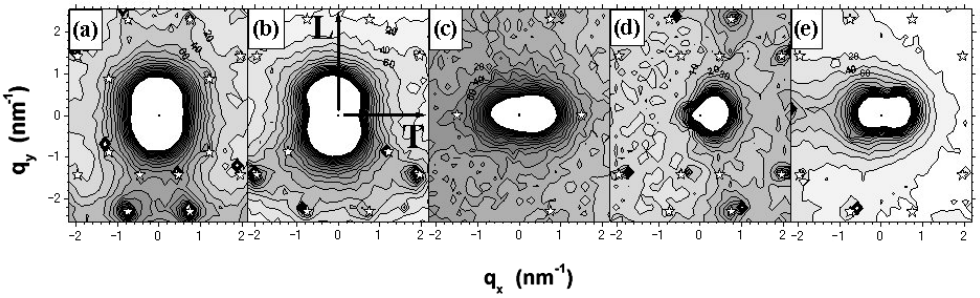

Figure 5. The observed diffuse scattering around (a) $10\bar{3}\bar{3}0$, (b) $30\bar{4}\bar{4}0$, (c) $0\bar{1}\bar{2}\bar{2}0$, (d) $1\bar{1}\bar{3}\bar{2}0$ and (e) $1\bar{2}\bar{5}\bar{4}0$ Bragg reflections at 8.103 keV. Absolute intensity is given in electron units. The open stars present the ideal positions for the weak Bragg reflections.

Q_x, Q_y and Q_z are set to measure the diffuse scattering three dimensionally as shown in figure 4. Figures 5(a)–(e) show the distributions of the diffuse scattering on a quasiperiodic plane around $10\bar{3}\bar{3}0$ (A in figure 4), $30\bar{4}\bar{4}0$ (B in figure 4), $0\bar{1}\bar{2}\bar{2}0$ (C in figure 4), $1\bar{1}\bar{3}\bar{2}0$ (D in figure 4) and $1\bar{2}\bar{5}\bar{4}0$ (E in figure 4) Bragg reflections at 8.103 keV, respectively. The quantitative diffuse intensities are corrected by measuring the standard Ni polycrystal. After data corrections, Thomson scattering (electron units per atom) is determined as the absolute value and the incoherent Compton scattering is subtracted using the calculated values. Numbers in contour maps are in electron units per atom. The resolutions of each Bragg reflection are given by the small dots in the center of the contour maps. By measurements along the periodic direction, we found the diffuse scattering distributed only on quasiperiodic planes, and not in the periodic direction. For instance, the correlation length is 4 nm along the quasiperiodic direction and is 8 nm along the periodic one. Compared with $Al_{72}Ni_{20}Co_8$, the distributions of the zone-centered diffuse scattering in $Al_{72}Ni_{18}Fe_{10}$ were anisotropic. Nevertheless, $Al_{72}Ni_{18}Fe_{10}$ had no 'random phason strain', as shown in figure 3. Furthermore, weak Bragg reflections were shifted a little from the ideal positions, which are indicated by the open stars in figures 5(a)–(e). Peak shifts had no $|\mathbf{G}^{\perp}|$ dependence. In principle, peak shifts, which are proportional to $|\mathbf{G}^{\perp}|$ values, are caused by 'phason strain'. In addition,

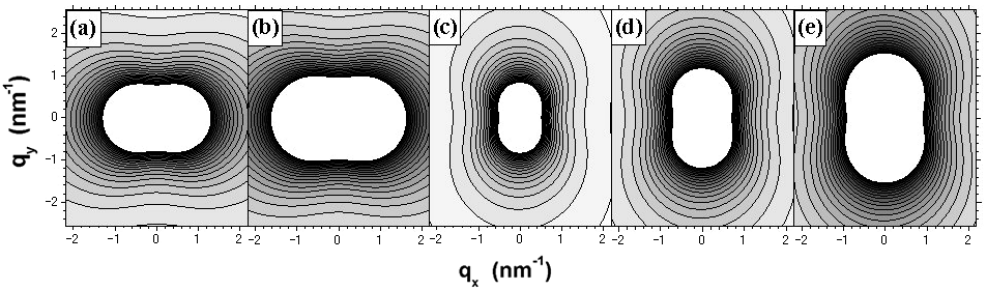

Figure 6. The calculated thermal diffuse scattering around (a) $10\bar{3}\bar{3}0$, (b) $30\bar{4}\bar{4}0$, (c) $0\bar{1}\bar{2}\bar{2}0$, (d) $1\bar{1}\bar{3}\bar{2}0$ and (e) $1\bar{2}\bar{5}\bar{4}0$ Bragg reflections.

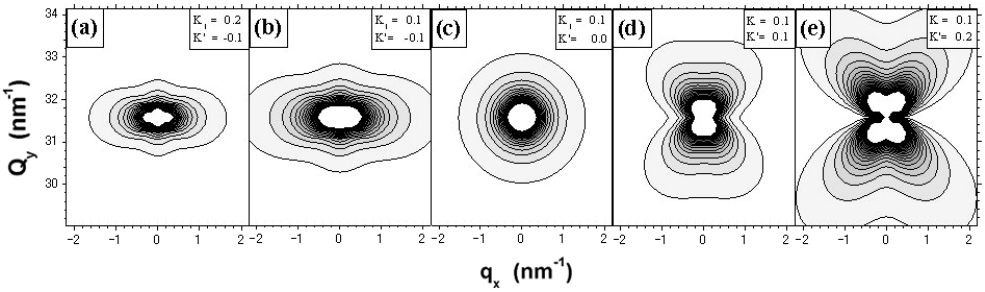

Figure 7. Theoretical phasonic diffuse scattering around $10\bar{3}\bar{3}0$ Bragg reflections using (a) $K_1 = 0.2$ and $K' = -0.1$, (b) $K_1 = 0.1$ and $K' = -0.1$, (c) $K_1 = 0.1$ and $K' = 0$, (d) $K_1 = 0.1$ and $K' = 0.1$ and (e) $K_1 = 0.1$ and $K' = 0.2$. K_1 is the phason elastic constant. Anisotropic distributions are enhanced by the coupling constant between phonon and phason, K'.

the distributions of the diffuse scattering around $0\bar{1}\bar{2}\bar{2}0$ and $1\bar{1}\bar{3}\bar{2}0$ Bragg reflections became asymmetric along the radial direction. These imply that a static strain derived from a defect or SE associated with SRO occurs in the as-quenched sample in spite of a high-quality quasicrystal.

There are four kinds of diffuse scattering to explain the observed ones: TDS, PDS, HDS and the SRO diffuse scattering with SE. Distributions of TDS are calculated by equations (10) and (12). The calculation results on a quasiperiodic plane ($q_3 = 0$) are shown in figures 6(a)–(e). In the actual calculation, we use λ ($= 0.5736$) and μ ($= 0.8845$) values in $Al_{71}Ni_{16}Co_{13}$ single quasicrystals [23]. The calculated TDS distributes along a transverse (T-) direction. Obviously, the observed diffuse scattering was distributed along a longitudinal (L-) direction in all contour maps as shown in figures 5(a)–(e). The calculated distributions of TDS cannot reproduce the observed ones. Next, we investigate PDS contributions. We calculated the PDS described by equations (11) and (12). On $Q_z = 0$, elastic constants are reduced to λ, μ, K_1 and K'. Figures 7(a)–(e) exhibit the theoretical PDS distributions around the $10\bar{3}\bar{3}0$ Bragg reflection satisfying the conditions in equation (13). With any combination of K_1 and K', the calculated PDS distributions contradict the observed ones. In principle, the diffuse scattering derived from pure phason contributions is isotropic on a decagonal quasicrystal. A coupling between phonon and phason can modify the distributions to become anisotropic.

Another approach to analyze the strains is to investigate the q dependence of the diffuse scattering. In fact, the q dependence of the scattered intensity contains significant information about lattice distortions. Theoretically, q^{-2} dependence is seen in TDS, HDS and PDS, which

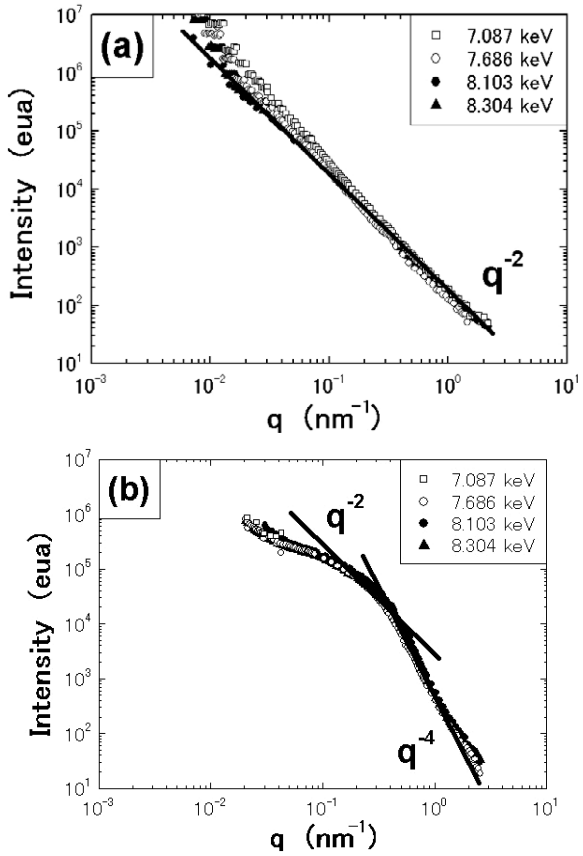

Figure 8. The scattered intensities at each incident energy versus q around the $30\bar{4}\bar{4}0$ Bragg reflection along (a) transverse (T-) and (b) longitudinal (L-) directions. Measurement regions are displayed in figure 5(b). Only along the L-direction, the scattered intensity shows q^{-4} dependence, which is derived from the strongly distorted regions.

are given by equations (5), (6) and (11), respectively. Thus, we examine the q relationship of the diffuse scattering along T- and L-directions, whether it obeys a power law or not. Line scans along T- and L-directions are drawn in figure 5(b). Figure 8(a) shows q^{-2} decay along T-detection around $30\bar{4}\bar{4}0$ Bragg reflection. Here, the scattered intensity at small q region (<0.1 nm^{-1}) is regarded as the tail of Bragg reflection. In contrast to the q^{-2} dependence, q^{-4} decay appears only along the L-direction (figure 8(b)). q^{-4} dependence is an inherent property for HDS [20]. In a crystal, strongly distorted regions provide q^{-4} dependence along the radial direction, though TDS has only q^{-2} dependence. There are no reports associated with q^{-4} dependence in a quasicrystal. The diffuse intensities along the T-direction indicated the incident energy dependence, although the diffuse intensities along the L-direction did not vary (figure 8(b)). For instance, the quantitative diffuse intensity at 8.103 keV provided the minimum values as shown in figure 8(a). This is because $|f_{\mathrm{Ni}} - f_{\mathrm{Fe}}|$ becomes almost zero at 8.103 keV and $\alpha_{\mathrm{Ni-Fe}}(\mathbf{q})$ is negligible at this incident energy. If the SRO diffuse scattering of $\alpha_{\mathrm{Al-Ni}}(\mathbf{q})$ and $\alpha_{\mathrm{Fe-Al}}(\mathbf{q})$ is rather smaller than that of $\alpha_{\mathrm{Ni-Fe}}(\mathbf{q})$, $I^{\mathrm{TDS+HDS}}$ distributes mainly at 8.103 keV. In fact, the diffuse intensity only at 8.103 keV obeyed q^{-2} dependence as shown in figure 8(a).

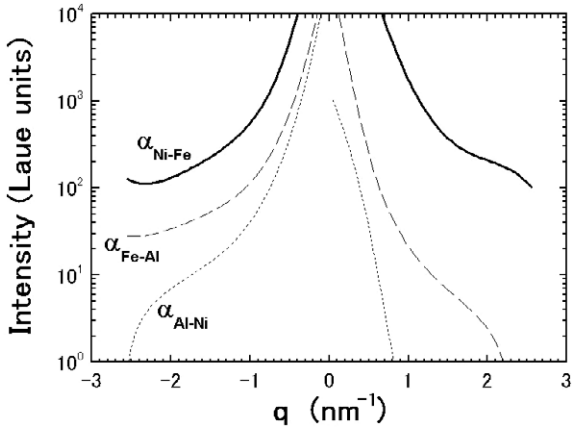

Figure 9. Three kinds of pair-correlation functions, $\alpha_{\mathrm{Al-Ni}}(\mathbf{q})$, $\alpha_{\mathrm{Ni-Fe}}(\mathbf{q})$ and $\alpha_{\mathrm{Fe-Al}}(\mathbf{q})$, in Laue units per atom. The q-region is the longitudinal direction in the center of the $30\bar{4}\bar{4}0$ Bragg reflection.

We estimate atomic SRO quantitatively considering intensity modulations at each incident energy. Apart from the calculated PDS, we assume that the scattered intensities consist of I^{SRO}, I^{SE} and $I^{\mathrm{TDS+HDS}}$. By self-consistent calculation using the Monte Carlo (MC) method, we compare the observed diffuse scattering with the calculated I^{SRO} and $I^{\mathrm{TDS+HDS}}$. The calculated $\log\{\alpha(\mathbf{q})\}$ is described as $k_0 + k_1 q + k_2 q^2 + k_3 q^3 + k_4 q^4$, while the calculated $I^{\mathrm{TDS+HDS}}$ is proportional to $|\bar{f}(\mathbf{Q}, E)|^2/q^2$. The convergence condition for the calculation is a reliability factor given by $R = \sum |\log(I^{\mathrm{cal}}) - \log(I^{\mathrm{obs}})| / \sum |\log(I^{\mathrm{obs}})|$. Then, $I^{\mathrm{TDS+HDS}}$ around $30\bar{4}\bar{4}0$ is found to be $0.2|\bar{f}|^2/q^2$ along the radial direction. I^{SRO} is obtained by subtracting the calculated $I^{\mathrm{TDS+HDS}}$ from the total diffuse scattering. Furthermore, we decomposed I^{SRO} into three $\alpha(\mathbf{q})$, which represent the three kinds of pair-correlation function in equation (7). Since $|\Delta f|^2$ depends ultimately on the incident energies as shown in figure 1, an advantage of $|\Delta f|^2$ by anomalous x-ray scattering makes it possible to separate into three $\alpha(\mathbf{q})$ analytically. Equation (7) is rewritten as

$$\begin{bmatrix} I^{\mathrm{SRO}}(\mathbf{Q}, E_1) \\ I^{\mathrm{SRO}}(\mathbf{Q}, E_2) \\ I^{\mathrm{SRO}}(\mathbf{Q}, E_3) \end{bmatrix} = \begin{bmatrix} \xi_{\mathrm{AB}}(\mathbf{Q}, E_1) & \xi_{\mathrm{BC}}(\mathbf{Q}, E_1) & \xi_{\mathrm{CA}}(\mathbf{Q}, E_1) \\ \xi_{\mathrm{AB}}(\mathbf{Q}, E_2) & \xi_{\mathrm{BC}}(\mathbf{Q}, E_2) & \xi_{\mathrm{CA}}(\mathbf{Q}, E_2) \\ \xi_{\mathrm{AB}}(\mathbf{Q}, E_3) & \xi_{\mathrm{BC}}(\mathbf{Q}, E_3) & \xi_{\mathrm{CA}}(\mathbf{Q}, E_3) \end{bmatrix} \begin{bmatrix} \alpha_{\mathrm{AB}}(\mathbf{q}) \\ \alpha_{\mathrm{BC}}(\mathbf{q}) \\ \alpha_{\mathrm{CA}}(\mathbf{q}) \end{bmatrix}. \tag{14}$$

The difference of atomic scattering factor is re-defined as $\xi_{ij}(\mathbf{Q}, E_n) = x_i x_j |f_i(\mathbf{Q}, E_n) - f_j(\mathbf{Q}, E_n)|^2$. Using the inverse matrix of $\xi_{ij}(\mathbf{Q}, E_n)$ coefficients, $\alpha_{\mathrm{Al-Ni}}(\mathbf{q})$, $\alpha_{\mathrm{Ni-Fe}}(\mathbf{q})$ and $\alpha_{\mathrm{Fe-Al}}(\mathbf{q})$ in Laue units per atom are calculated exactly at each incident energy (figure 9). The q region in figure 9 corresponds to the L-direction in the center of the $30\bar{4}\bar{4}0$ Bragg reflection. The inverse matrix method was valid for $Al_{72}Ni_{20}Co_8$, whose diffuse shapes are so complicated and anisotropic [24]. The classic least-square method cannot decompose the complicated SRO diffuse scattering into the partial diffuse intensities at all. We emphasize that atomic SRO exists in a decagonal quasicrystal and the decomposed partial diffuse intensities are asymmetric along the radial directions due to atomic SE. In particular, atomic SE is enhanced in $\alpha_{\mathrm{Al-Ni}}(\mathbf{q})$ and $\alpha_{\mathrm{Fe-Al}}(\mathbf{q})$. In addition, SRO between transition metals, that is, $\alpha_{\mathrm{Ni-Fe}}(\mathbf{q})$, is larger than other pair-correlation functions.

Table 1. Normalized $|\bar{f}|^2|\mathbf{G}|^2$ values of Bragg reflections. These are proportional to intensities of thermal diffuse scattering.

	$10\bar{3}\bar{3}0$	$30\bar{4}\bar{4}0$	$0\bar{1}\bar{2}20$	$1\bar{1}\bar{3}20$	$1\bar{2}\bar{5}40$
$\|\bar{f}\|^2$	113.7	64.5	176.4	129.7	81.2
$\|\mathbf{G}\|^2$	997.2	2610.8	275.6	721.6	1889.2
$\|\bar{f}\|^2\|\mathbf{G}\|^2$	0.673	1	0.289	0.555	0.910

5. Monte Carlo simulations

It is quite difficult to calculate the SRO diffuse scattering at the zone center, because we cannot obtain contributions both of TDS and HDS strictly. Nevertheless, we can estimate that $I^{\mathrm{TDS+HDS}}$ is $0.2|\bar{f}|^2/q^2$ around $30\bar{4}\bar{4}0$ by the above calculations. Approximately, $I^{\mathrm{TDS+HDS}}$ is proportional to $|\bar{f}|^2|\mathbf{G}|^2/q^2$. Therefore, $I^{\mathrm{TDS+HDS}}$ of $10\bar{3}\bar{3}0$, $0\bar{1}\bar{2}20$, $1\bar{1}\bar{3}20$ and $1\bar{2}\bar{5}40$ Bragg reflections are smaller than that of $30\bar{4}\bar{4}0$ (table 1). Therefore, we calculate the SRO diffuse scattering qualitatively neglecting TDS and HDS. Also, atomic SE is ignored, since SE calculation is impossible on a quasiperiodic lattice. For simplicity, only one correlation between Al and TM (transition metal) is introduced in the simulations using the observed data at 8.103 keV ($|f_{\mathrm{Ni}} - f_{\mathrm{Fe}}| \cong 0$), where $\alpha_{\mathrm{Ni-Fe}}(\mathbf{q})$ becomes almost zero for the null Laue case. This is a big advantage of anomalous x-ray scattering, where the simulations are treated as a binary alloy system.

MMC (Metropolis Monte Carlo) simulations are carried out using the experimentally obtained SRO diffuse intensities at 8.103 keV. Here, the MMC method avoids the MC simulation being trapped in a local energy minimum [25]. The entire process is repeated over MC steps until a ground state is achieved. Therefore, the SRO parameters are optimized by simulated annealing. Firstly, MMC simulations on the quasiperiodic lattice were applied to an $Al_{72}Ni_{20}Co_8$ quasicrystal [24]. The quantitative analysis of atomic SRO in a quasicrystal was carried out using the SRO diffuse scattering around superstructure reflections. It was also found that the MMC simulations diverge easily if the simulations are carried out without the SRO parameters. Thus, the SRO parameters were regarded as a good constraint for the MMC simulations, although the SRO parameters are merely one-dimensional reduced parameters. The SRO parameters obtained by the circular average in the shell are similar to the radial distribution function in liquids or amorphous materials. Exponential decay of the SRO parameter as a function of atomic distance represents the correlation length.

In this study, we apply the MMC simulations to the zone-centered diffuse scattering for the first time. The MMC simulations are performed on the $Q_z = 0$ plane. Thus, two-dimensional quasiperiodic lattices ($z = 1/4, 3/4$) are not distinguished from each other. Atomic positions are provided as shown in figures 10(a) and (b). Occupation domains in figures 10(c) and (d) can generate two kinds of columnar clusters. The closed and open circles reveal atoms at $z = 1/4$ and $z = 3/4$, respectively. The circles in figures 10(a) and (b) indicate 2 nm diameter for comparison. Two kinds of clusters are similar to the images observed in $Al_{70}Ni_{15}Fe_{15}$ by HAADF-STEM [7]. In the MMC simulations, an Al atom is put on the origin and is fixed over the MC steps. The range of radius in the mth shell, $\mathbf{R}_m$, is up to 6.0 nm. Total lattice sites of TM atoms are 865. The selected sites are reduced to 47 shells along the radial direction. Data are collected for 5×10^5 MC steps.

The detailed algorithm was described in previous studies [24, 26]. The MC simulations are divided into four steps. (i) Before MMC simulations, all $\alpha(\mathbf{R}_m)$ values are set to be zero. This means that an initial atomic arrangement is completely random. (ii) The SRO

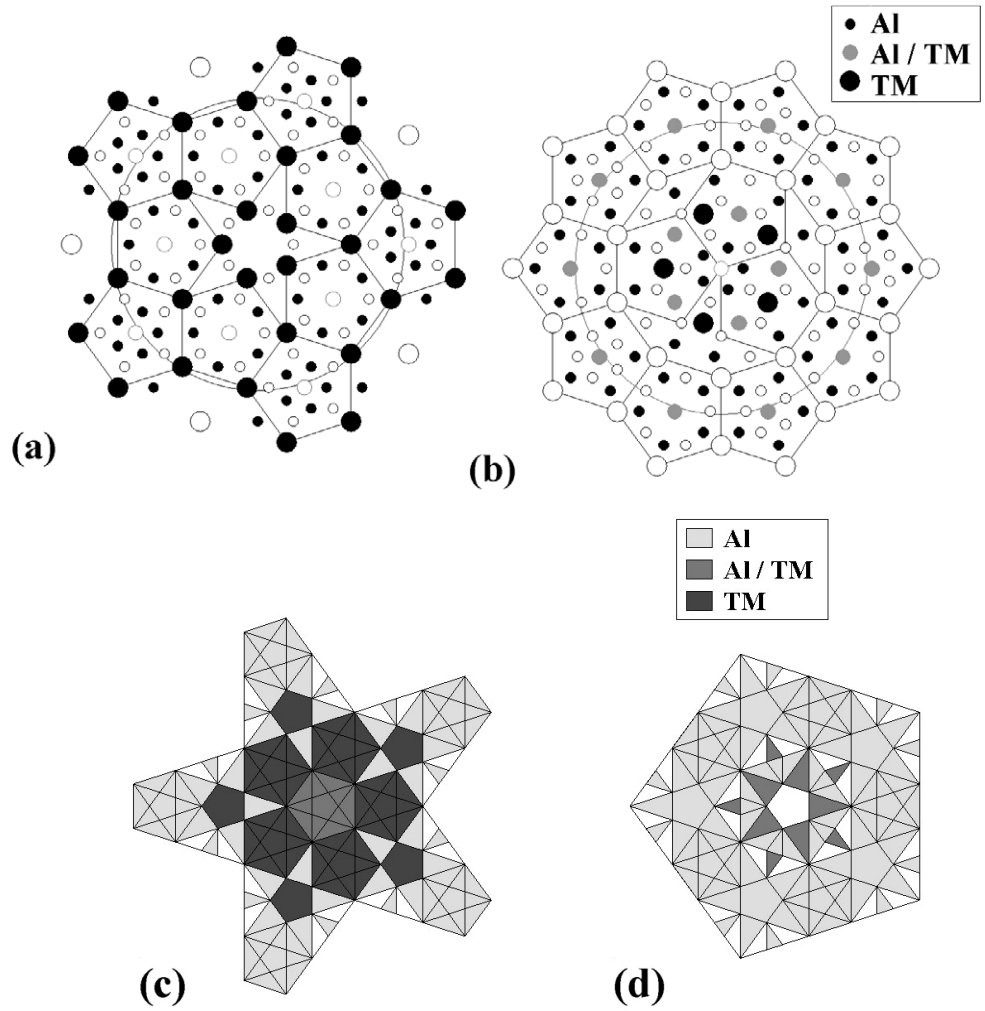

Figure 10. Two kinds of 2 nm diameter columnar cluster: (a) a star-type cluster; (b) a decagon-type cluster. Two circles exhibit 2 nm diameter. The closed and open circles reveal atoms at $z = 1/4$ and $z = 3/4$, respectively. The occupation domains are located at (a) (1/5, 1/5, 1/5, 1/5, 1/4) and (b) (2/5, 2/5, 2/5, 2/5, 1/4) in the five-dimensional decagonal lattice, respectively.

parameters in the mth shell are provided randomly at every MC cycle. (iii) Using randomly generated $\alpha(\mathbf{R}_m)$ in the mth shell, the SRO diffuse scattering is calculated by equation (2). (iv) The calculated diffuse intensity, $\alpha^{\mathrm{cal}}(\mathbf{q})$, is compared with the observed diffuse scattering, $\alpha^{\mathrm{obs}}(\mathbf{q})$, at 8.103 keV. The reliability factor (R-factor) is introduced to investigate the matching factor between $\alpha^{\mathrm{cal}}(\mathbf{q})$ and $\alpha^{\mathrm{obs}}(\mathbf{q})$. If the R-factor during a present MC cycle is smaller than that of the previous one, the generated $\alpha(\mathbf{R}_m)$ in this cycle is replaced by the previous one. Consequently, the SRO parameter for better matching is determined by the R-factor at the MC cycles. In step (iv), one MC cycle finishes. Back to step (ii), the next MC cycle starts. The R-factor is expressed by

$$R = \sum \frac{|\alpha^{\mathrm{cal}}(\mathbf{q}) - \alpha^{\mathrm{obs}}(\mathbf{q})|}{|\alpha^{\mathrm{obs}}(\mathbf{q})|}. \tag{15}$$

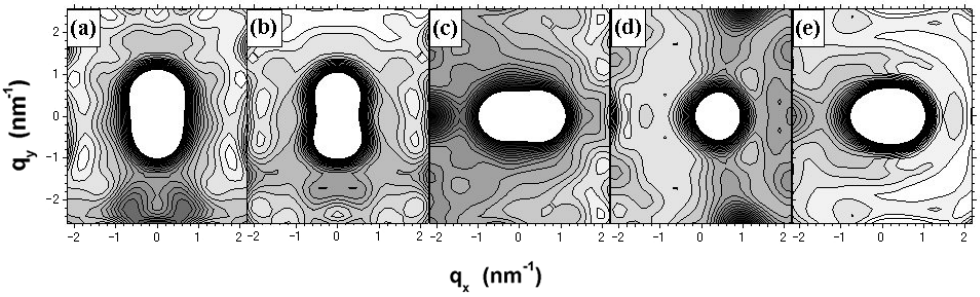

Figure 11. The simulated SRO diffuse scattering around (a) $10\bar{3}\bar{3}0$, (b) $30\bar{4}\bar{4}0$, (c) $0\bar{1}\bar{2}\bar{2}0$, (d) $1\bar{1}\bar{3}\bar{2}0$ and (e) $1\bar{2}\bar{5}\bar{4}0$ Bragg reflections by the Metropolis Monte Carlo method. In the simulations, the observed SRO diffuse scattering at 8.103 keV and SRO parameters are used.

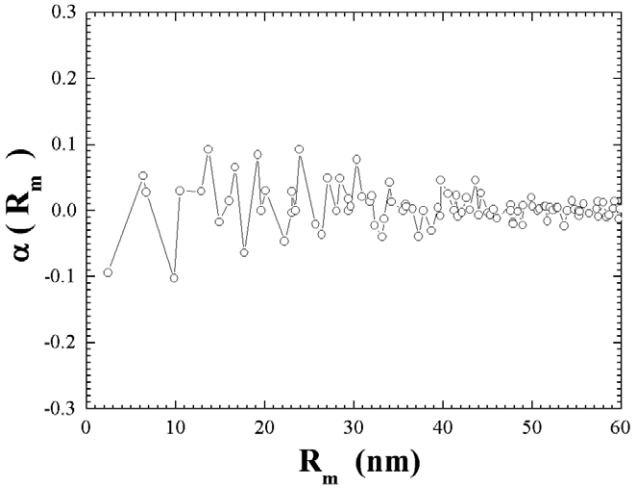

Figure 12. The SRO parameters of an Al–transition metal pair are optimized qualitatively by the Metropolis Monte Carlo method.

Figures 11(a)–(e) show the MMC simulation results. Without considering TDS, HDS and SE, the *R*-factor remains 30%. Even though the above rough assumptions are considered in the simulation, the calculated distributions of the SRO diffuse scattering almost coincide with the observed ones. At the same time, the SRO parameters are also optimized qualitatively by the MMC simulations. $\alpha(\mathbf{R}_m)$ of an Al–TM pair is shown in figure 12. $\alpha(\mathbf{R}_m)$ values are normalized using the relation $\alpha(\mathbf{0}) \equiv 1$. Without using the above relation, the inverse Fourier transform of $\alpha(\mathbf{q})$ over the whole reciprocal space should be required in order to obtain the SRO parameters. This is because a quasicrystal has no first Brillouin zone.

6. Remarks

The anisotropic distributions of the observed diffuse scattering in the as-quenched $Al_{72}Ni_{18}Fe_{10}$ quasicrystal are not reproduced by the theoretical PDS calculations, which are described by 'phason modes'. We show that the anisotropy originates from the atomic SRO by (i) intensity modulations in anomalous x-ray scattering, (ii) SRO decomposition into three atomic pairs and (iii) MMC simulations using the SRO parameters. In (ii), the SRO between Ni and Fe,

$\alpha_{\mathrm{Ni-Fe}}(\mathbf{q})$, is the largest among the atomic pairs. The observed diffuse intensities along the T-direction were minimum at 8.103 keV ($|f_{\mathrm{Ni}} - f_{\mathrm{Fe}}| \cong 0$), since the largest $\alpha_{\mathrm{Ni-Fe}}(\mathbf{q})$ contribution disappeared at this incident energy. The decomposed SRO diffuse scatterings distribute asymmetrically along the L-direction. This is caused by atomic SE. In (iii), SRO between Al and TM can reproduce the anisotropic distributions qualitatively by the MMC simulations. MMC simulations are applied to the zone-centered diffuse scattering in a quasicrystal for the first time. This is the first step to analyze a disordered state in a complex material. The SRO parameters are regarded as a good constraint in the simulations. Without them, the simulations diverge quickly.

The experimental results about lattice distortions are too complex to be systematically explained. q^{-4} dependence of the diffuse scattering along the L-direction remains unclear and has to date no theoretical explanation. The diffuse scattering is strongly dependent on strains such as SE or lattice distortions.

Acknowledgments

We appreciate helpful discussions with Professor Y Ishii of Chuo University, Professor E Abe of the University of Tokyo, Professor H Takakura of Hokkaido University and Dr K Saitoh of Nagoya University. Also, we would like to thank Dr H Nakao of Tohoku University and Dr Y Wakabayashi of the Photon Factory for experimental support.

References

[1] Tsai A P, Inoue A and Masumoto T 1989 *Mater. Trans. JIM* **30** 150
[2] Black P J 1955 *Acta Crystallogr.* **8** 43
Black P J 1955 *Acta Crystallogr.* **8** 175
[3] Saito K, Sugiyama K and Hiraga K 2000 *Mater. Sci. Eng.* **294–296** 279
[4] Saito M, Tanaka M, Tsai A P, Inoue A and Masumoto T 1992 *Japan. J. Appl. Phys.* **31** L109
[5] Tsuda K, Saito M, Terauchi M, Tanaka M, Tsai A P, Inoue A and Masumoto T 1993 *Japan. J. Appl. Phys.* **32** 129
[6] Hiraga K, Yubuta K and Park K 1996 *J. Mater. Res.* **11** 1702
[7] Saitoh K, Tsuda K, Tanaka M and Tsai A P 1999 *Japan. J. Appl. Phys.* **38** L671
[8] Weidner E, Frey F, Lei J-L, Pedersen B, Paulmann C and Morgenroth W 2004 *J. Appl. Crystallogr.* **37** 802
[9] Yamamoto K, Matsuoka S, Abe H and Matsuo Y 2007 in preparation
[10] Ice G E, Sparks C J, Habenshuss A and Shaffer L B 1992 *Phys. Rev. Lett.* **68** 863
[11] Abe H, Matsuo Y, Saitoh H, Kusawake T, Ohshima K and Nakao H 2000 *Japan. J. Appl. Phys.* **39** L1111
[12] Abe H, Saitoh H, Ueno T, Nakao H, Matsuo Y, Ohshima K and Matsumoto H 2003 *J. Phys.: Condens. Matter* **15** 1665
[13] Lubensky T C, Socolar J E S, Steinhardt P J, Bancel P A and Heiney P A 1986 *Phys. Rev. Lett.* **57** 1440
[14] Henley C L 1988 *J. Phys. A: Math. Gen.* **21** 1649
[15] de Boissieu M, Boudard M, Hennion B, Bellissent R, Kycia S, Goldman A, Janot C and Audier M 1995 *Phys. Rev. Lett.* **75** 89
[16] Abe H, Tamura N, Le Bolloc'h D, Moss S C, Matsuo Y, Ishii Y and Bai J 2000 *Mater. Sci. Eng.* A **294–296** 299
[17] Moss S C 1995 *Mater. Res. Soc. Symp. Proc.* **376** 675
[18] Hashimoto S 2000 *Acta Crystallogr.* A **56** 85
[19] Wooster W A 1997 *Diffuse X-ray Reflections from Crystals* (New York: Dover) republished in 1997
[20] Dederichs P H 1973 *J. Phys. F: Met. Phys.* **3** 471
[21] Ishii Y 1992 *Phys. Rev.* B **45** 5228
[22] Ishii Y 2000 *Mater. Sci. Eng.* **294–296** 377
[23] Chernikov M A, Ott H R, Bianchi A, Migliori A and Darling T W 1998 *Phys. Rev. Lett.* **80** 321
[24] Abe H 2007 *Japan. J. Appl. Phys.* submitted
[25] Metropolis N, Rosenbluth A W, Rosenbluth M N and Teller A H 1953 *J. Chem. Phys.* **21** 1087
[26] Abe H 2007 *J. Phys. Soc. Japan* **76** 094601